DOI: 10.1021/ma900110w

Macromolecules
NOTE

Cylindrical Microdomain Orientation of PS-*b*-PMMA on the Balanced Interfacial Interactions: Composition Effect of Block Copolymers

Du Yeol Ryu,*,† Sujin Ham,† Eunhye Kim,† Unyong Jeong,‡ Craig J. Hawker,§ and Thomas P. Russell⊥

†*Department of Chemical Engineering and* ‡*Department of Materials Science and Engineering and Active Polymer Center for Pattern Integration, Yonsei University, Seoul 120-749, Korea,* §*Material Research Laboratory and Departments of Materials, Chemistry and Biochemistry, University of California, Santa Barbara, California 93016, and* ⊥*Department of Polymer Science & Engineering, University of Massachusetts, Amherst, Massachusetts 01003*

Received January 18, 2009
Revised Manuscript Received April 2, 2009

Introduction

Block copolymer (BCP) self-assembly has recently attracted significant interest, since the resultant bulk and thin film morphologies offer ideal platforms for the generation of nanoscopically ordered patterns in a range of the promising applications.[1−5] The bulk phase behavior is classically dictated by the molecular weight (N), interaction parameter (χ), the relative composition (Φ), and chain rigidity.[6−8] As for thin films, however, interfacial interactions play an important role in influencing the morphology and orientation of the BCP microdomains,[9,10] allowing the desired nanopatterns or arrays.[11−14] Preferential wetting of one block component with the substrate or difference in the surface energy of two components will lead to a parallel microdomain orientation to the substrate,[15−19] while the balanced interfacial interactions at surface (the so-called neutral surface) favors a microdomain orientation normal to the film surface.[20,21]

To address this challenge for the perpendicular microdomain orientation, various strategies have been developed to control microdomain orientations of BCP films including surface modification,[22−28] external fields,[29,30] solvent annealing,[31,32] and surface patterning.[33,34] The simple approach to surface modification using random or functional copolymers has proven to be versatile and extendable to a wide range of polymeric materials because the balanced interfacial interactions can be tuned by controlling the relative composition of copolymers. For example, using hydroxyl-functionalized P(S-*r*-MMA) copolymer, characteristic surface properties ranging from PS to PMMA can be obtained depending upon PS/PMMA composition.[20,21,35,36] The dewetting behaviors of PS and PMMA homopolymers on the various random copolymer brushes showed that the interfacial interactions on the substrate were balanced at a styrene fraction of ~0.58 in the P(S-*r*-MMA).[20]

Recent studies on the surface neutrality for PS-*b*-PMMA have shown that, when interfacial interactions are balanced ($\Delta\gamma = |\gamma_{As} - \gamma_{Bs}|$ close to 0) where $\Delta\gamma$ is the difference in interfacial energies between components A and B with the substrate (s) for the random copolymer brushes, only the film thickness around the lattice period (L_0) controls the microdomain orientation.[27] Detailed studies on film thicknesses favoring a microdomain orientation normal to the film surface indicate that the optimal conditions for the balanced interfacial interactions (the so-called neutrality in random copolymer) are found when X_S (styrene mole fraction) = 0.64, whereas for the lamellar microdomains X_S = 0.55. Nealey et al. also reported the perpendicular window at selected thicknesses for lamella- and cylinder-forming PS-*b*-PMMAs as a function of PS mole fraction for various random copolymer brush and mat.[37] These studies in addition to the prior efforts provide a straightforward set of guidelines to control microdomain orientation of PS-*b*-PMMA.

Here, we discuss the compositional asymmetry effects on the microdomain orientations of cylinder-forming PS-*b*-PMMA by the thickness window where the cylindrical microdomains orient normal to the film surface. The greater the asymmetry of the PS-*b*-PMMA, the greater is the tendency for the microdomain orientation normal to the neutral surfaces, while the optimal conditions for the balanced interfacial interactions holds the same X_S = 0.64 for the random copolymers.

Experimental Section

Hydroxyl (HO)-functionalized P(S-*r*-MMA), with X_S ranging from 0.34 to 0.85, were synthesized by a nitroxide-mediated living free radical polymerization.[20,38] Number-average molecular weights (M_n) and polydispersity (M_w/M_n) of P(S-*r*-MMA)s were ~10 000 g/mol and less than 1.30, respectively. R*x* defines the S mole fractions in the random copolymers.[27] Three cylinder-forming PS-*b*-PMMA-*y*, having PS volume fractions (Φ_{PS}) of 0.72, 0.76, and 0.80 where *y* is the volume percentage of PS, were synthesized by the sequential anionic polymerization of styrene and methyl methacrylate in tetrahydrofuran (THF) at −78 °C in the presence of LiCl (high purity, Aldrich). M_n and M_w/M_n of the PS-*b*-PMMA copolymers were determined by size-exclusion chromatography (SEC) with the multiangle laser light scattering (MALLS), as listed in Table 1.

The surface modification by HO-P(S-*r*-MMA) was accomplished by thermally annealing thin films on cleaned Si wafers under vacuum at 170 °C, well above the glass transition temperatures (T_g) of both PS (100 °C) and PMMA (115 °C) for 3 days, resulting in polymer chain brushes on the substrate after repeated rinsing with toluene to remove the unreacted polymer chains. The brush thickness of P(S-*r*-MMA)s was measured to be ~4.6 ± 0.2 nm by ellipsometry (SE MG-1000, Nanoview Co.) at an incidence angle of 70°. Scanning force microscopy (SFM; Dimension 3100, Digital Instrument Co.) was operated in the tapping mode to investigate the surface morphology of the BCP thin films, with the PMMA microdomains appearing brighter in phase due to the viscoelastic contrast between the two block components.

Grazing-incidence small-angle X-ray scattering (GISAXS) experiments were performed at the 4C2 beamline in the Pohang Accelerator Laboratory (PAL), Pohang, Korea. The operating conditions were set to a wavelength of 0.138 nm and a sample-to-detector distance of 2.5m. The samples were mounted in a vacuum chamber, and the incident angles were set at 0.16° or 0.18°, which are above the critical angle (0.135°) of PS-*b*-PMMA thin films. To enhance the X-ray contrast, the PMMA component was selectively removed by exposure to ultraviolet (UV) radiation and acetic acid treatment. Transmission small-angle X-ray scattering (SAXS; at 4C1 beamline) was used to characterize the morphologies of BCP in the bulk state.

*To whom correspondence should be addressed. E-mail dyryu@yonsei.ac.kr.

 Published on Web 05/04/2009

Table 1. Characteristics of Cylinder-Forming PS-*b*-PMMAs Used in This Study

sample code	PS volume fraction[a]	M_n[b]	M_w/M_n[b]	L_0[c] (nm)	⊥[d] on R62 (nm)	⊥ on R64 (nm)	⊥ on R66 (nm)
PS-*b*-PMMA-72	0.72	88 000	1.04	35.4	17.0−39.0	12.6−41.9	17.6−39.3
PS-*b*-PMMA-76	0.76	86 000	1.06	34.9	13.3−40.1	13.6−42.5	13.1−41.7
PS-*b*-PMMA-80	0.80	87 000	1.06	34.0	14.1−45.8	10.8−45.4	14.1−44.8

[a] PS volume fractions of PS-*b*-PMMA were calculated based on molar compositions by ^{1}H nuclear magnetic resonance (^{1}H NMR) with mass densities of two components (1.05 and 1.184 g/cm^3 for PS and PMMA, respectively). [b] Molecular weight (M_n) and polydispersity for PS-*b*-PMMA were characterized by size-exclusion chromatography (SEC) with the multiangle laser light scattering (MALLS). [c] Lattice periods (L_0 or *d*-spacing, $d = 2\pi/q_y^{max}$) for PS-*b*-PMMA were calculated based on the primary peaks (q_y^{max}) along the in-plane scattering in the GISAXS patterns. [d] The symbol ⊥ indicates the thickness range for the cylindrical microdomain orientation normal to the film surface on the substrates modified by R62, R64, and R66.

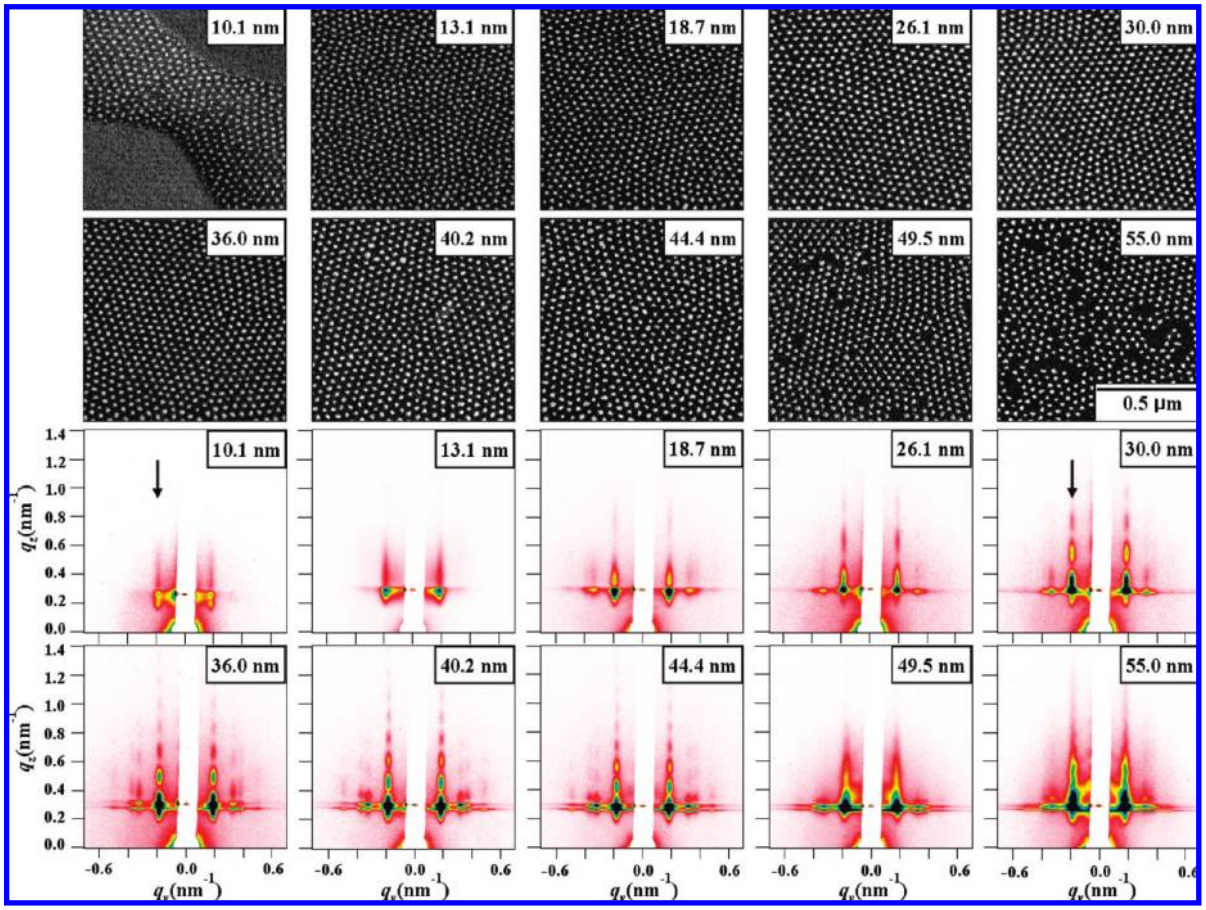

Figure 1. SFM phase images and the corresponding two-dimensional GISAXS patterns at incident angles of 0.16° (10.1 nm thickness) and 0.18° (the others) for thin films of cylinder-forming PS-*b*-PMMA-80 on the substrate modified by R64 (having a PS mole fraction of 0.64) at various film thicknesses after thermally annealing thin films at 170 °C for 24 h. To increase the scattering contrast, PMMA microdomains were removed from all thin film samples by UV exposure and subsequent rinsing with acetic acid. Arrows are drawn to compare the peak maxima.

Results and Discussion

Thin films of cylinder-forming PS-*b*-PMMA were spin-coated onto the substrates modified by various random copolymers. Figure 1 shows the SFM phase images selected for thin films of PS-*b*-PMMA-80 (PS volume fraction of 0.80) on R64 and the corresponding two-dimensional grazing-incidence small-angle X-ray scattering (GISAXS) patterns, after thermally annealing thin films at 170 °C for 24 h under vacuum. When the film thickness is 10.1 nm or less, the SFM images show that the cylindrical microdomains on the covered region are oriented normal to the film surface, but the others are featureless. Bearing in mind that the interactions of the block components with the substrate are nonfavorable, these results indicate that the BCP film dewets the substrate, yielding areas that are devoid of the PS-*b*-PMMA. As the film thickness increases, dewetting is retarded and the surface becomes stable. For films with thicknesses from 13.1 to 44.4 nm, the cylindrical microdomains of the PS-*b*-PMMA-80 are seen to orient normal to the film surface. However, for thin films with thicknesses ≥49.5 nm, the ordering and orientation of the cylindrical microdomains at the free surface degrade, since the influence of the balanced interfacial interactions from R64 diminishes and the PS component of lower surface energy tends to place at the top surface, consequently causing the microdomains to orient parallel to the film surface.

GISAXS patterns for the PS-*b*-PMMA-80 films on R64, where the PMMA block was selectively removed, are shown in Figure 1 along with the SFM images. In the scattering geometry, q_y is the scattering vector normal to the plane of incidence (parallel to the film surface), where the *d*-spacing is related to q_y by $d = 2\pi/q_y^{max}$. q_z is the scattering vector normal to the sample surface, defined as $q_z = (4\pi/\lambda)\sin\theta$, where λ is the wavelength of the X-rays and 2θ is the scattering angle. The scattering peaks for the 10.1 nm film show a lower intensity only for the first-order peak near $q_y^{max} = 0.185$ nm^{-1} at constant $q_z = 0.258$ nm^{-1} due to the partial orientation of the cylindrical microdomains normal to the film surface. This intensity of the first-order reflection increases and

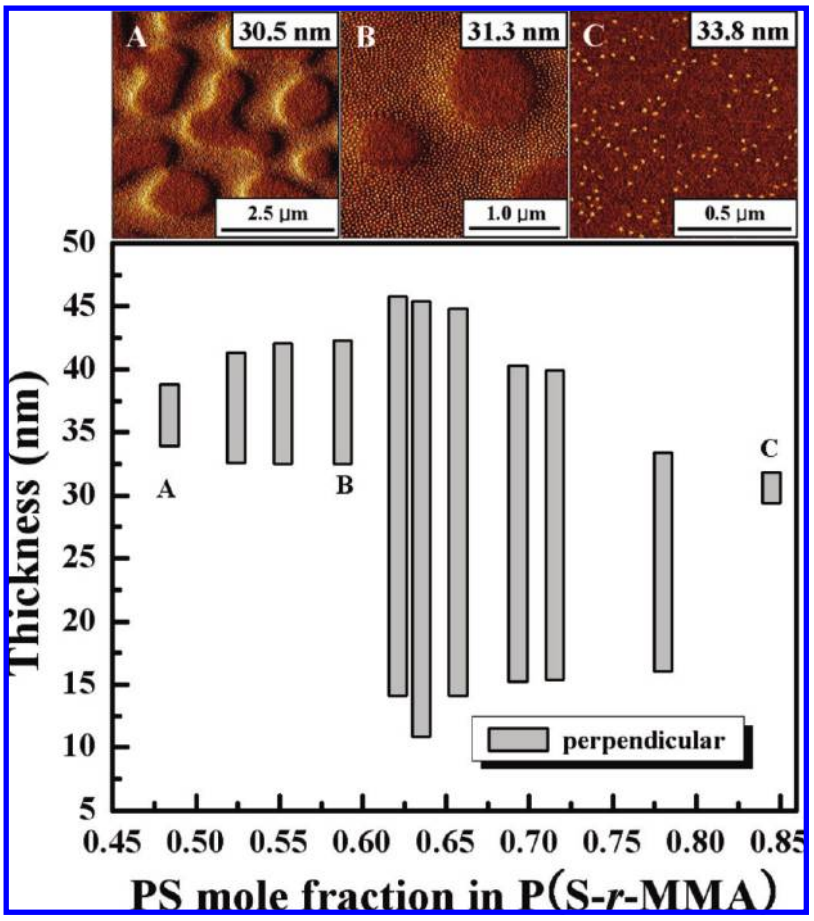

Figure 2. Thickness window for PS-*b*-PMMA-80, where the cylindrical microdomains orient normal to the film surface, as a function of S mole fraction (X_S) of random copolymers anchored to the substrate, X_S ranging from 0.34 to 0.85. The SFM phase images on the surface morphologies at A, B, and C points, taken out of thickness window, illustrate dewetting morphologies such as hole/islands, degraded ordering structures, as the nonperpendicular microdomain orientations in thin films.

higher-order peaks appear as the film thickness increases. GISAXS patterns for thin films with thicknesses ≤44.4 nm show a sharp first-order peak at $q_y^{max} = 0.185$ nm^{-1} along constant $q_z = 0.292$ nm^{-1} with higher-order peaks at $q_y = 0.321$, 0.370, and 0.489 nm^{-1} at scattering vector ratios of 1:$\sqrt{3}$:$\sqrt{4}$:$\sqrt{7}$ relative to a first-order peak, indicating a hexagonally packed arrays of cylindrical microdomain oriented normal to the film surface with a *d*-spacing of 34.0 nm ($d = 2\pi/q_y^{max}$). These results are in good agreement with the SFM results even when a dewetting of the film is observed. However, for films with thicknesses of 49.5 and 55.0 nm, the GISAXS patterns show not only Bragg rods associated with the microdomain orientation but also a ringlike scattering pattern arising from the random orientation of the microdomains. This thickness dependence of the microdomain orientations can be attributed to the commensurability between the films thickness and the lattice period (L_0).

The thickness window of PS-*b*-PMMA-80 where the cylindrical microdomains orient normal to the film surface was consequently determined as a function of X_S for random copolymers anchored to the substrate, where X_S ranges from 0.34 to 0.85, as shown in Figure 2. When $X_S < 0.48$, the cylindrical microdomains were oriented parallel to the film surface, regardless of the film thicknesses due to the preferential interactions of the PMMA block with the random copolymer brushes. For R48 to R59 ($X_S = 0.48-0.59$), the microdomains were found to orient normal to the film surface for a narrow thickness window, with the width of the thickness window increasing slightly with increasing X_S. A larger thickness window to obtain a microdomain orientation was observed for $X_S = 0.62-0.66$, with the largest thickness window (from 10.8 to 45.4 nm) occurring at $X_S = 0.64$, which represents the optimal conditions for the balanced interfacial interactions at this composition. Increasing X_S to 0.85 narrows the thickness window substantially (from 29.4 to 31.8 nm). For $X_S > 0.85$, the microdomains orient parallel to the film surface due to the enhanced interaction of PS block with the random copolymer brushes. The SFM images (in Figure 2) on the surface morphologies, taken out of thickness window, illustrate dewetting morphologies such as hole/islands, degraded ordering structures.

In comparison to a previous report on cylinder-forming PS-*b*-PMMA-72 studied,[27] it is noticeable for PS-*b*-PMMA-80 that the same optimal conditions for balanced interfacial interactions (the so-called neutrality condition) was observed in the current study for $X_S = 0.64$ ranging from $X_S = 0.62$ to 0.66 in the random copolymers. It should be also pointed out that, even in thin films of cylinder-forming PS-*b*-PMMA-76, the same optimal conditions were found at $X_S = 0.64$ in a similar manner. This result confirms that the optimal composition of the P(S-*r*-MMA) for the balanced interfacial interactions is equivalent to $X_S = 0.64$ as long as the cylindrical morphology is conserved, regardless of the relative compositions of PS-*b*-PMMA. Moreover, for thin films of a highly asymmetric cylinder-forming PS-*b*-PMMA-80, the more extensive compositional range of X_S from 0.48 to 0.85 as well as the larger thickness window in the vicinity of the neutral surfaces ($X_S \sim 0.64$) indicates that the cylindrical microdomain orientation normal to the neutral surfaces is favored for the more asymmetric PS-*b*-PMMA (the shorter PMMA).

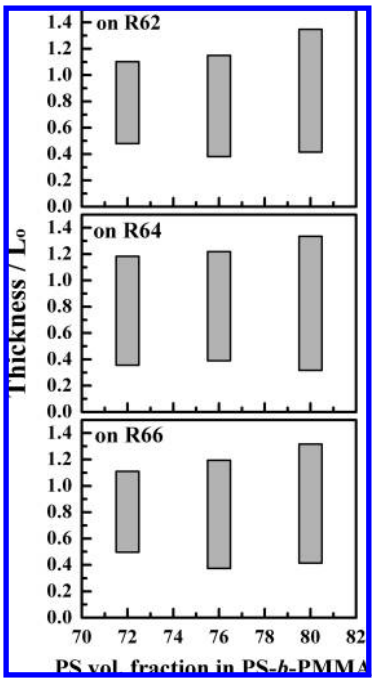

Figure 3. Thickness windows for the cylindrical microdomain orientation normal to the film surface as a function of PS volume fraction (0.72, 0.76, and 0.80) in cylinder-forming PS-*b*-PMMAs on the substrates modified by R62, R64, and R66, which are taken in the vicinity of the balanced interfacial interactions. The thicknesses are normalized by each lattice period (L_0 or *d*-spacing, $d = 2\pi/q_y^{max}$) for reasonable comparison.

According to the self-consistent-field (SCF) calculations by Wang et al.,[39,40] the microdomain orientation of BCP thin film on the neutral surface was demonstrated by two competing effects, as follows. The decrease of polymer density near surface can enhance the neutrality (or surface-induced compatibilization), which favors the perpendicular microdomain orientation. In contrast, the entropic preference for the short component associated with the location of chain ends adjacent to the short component favors the parallel microdomain orientation. In the case of asymmetric cylinder-forming PS-*b*-PMMA, the latter represents that the composition in the random copolymers depends on the block composition of PS-*b*-PMMA for the rebalanced interfacial interactions on the surface to compensate this entropic preference, which is inconsistent with our results that the same balanced interfacial interactions ($X_S = 0.64$ in the random copolymer) were observed for thin films of three different cylinder-forming PS-*b*-PMMAs. Accordingly, this phenomenon might be dominantly correlated to the enhanced neutrality by the decrease of polymer density near surface favoring the perpendicular microdomain orientation, which is in turn expected to be significant in the thin films of highly asymmetric cylinder-forming PS-*b*-PMMA due to the overall enrichment of junction points closer to short PMMA component on the surface.

Figure 3 summarizes the thickness windows as a function of PS volume fraction (0.72, 0.76, and 0.80) in the cylinder-forming PS-*b*-PMMAs on the substrates modified by three different random copolymers, R62, R64, and R66, which are taken in the vicinity of the balanced interfacial interactions. The thicknesses are normalized by L_0 for comparison and listed in Table 1. For all cylinder-forming PS-*b*-PMMAs in this study, the largest thickness window was found for thin films on R64. The compositional dependence of the cylinder-forming PS-*b*-PMMAs on the thickness windows indicates that the greater the asymmetry of the PS-*b*-PMMA, the larger is the thickness window. This behavior is more evident on the surfaces modified by R62 and R66 in a similar tendency.

Summary

The microdomain orientations in thin films of cylinder-forming PS-*b*-PMMAs, having PS volume fraction (Φ_{PS}) = 0.72, 0.76, and 0.80, were investigated as a function of film thickness and the composition of the P(S-*r*-MMA) anchored to the substrate. From the thickness window where the cylindrical microdomains orient normal to the film surface, a larger range of thickness windows was observed for $X_S = 0.62$ to 0.66, with $X_S = 0.64$ being the optimal conditions for the balanced interfacial interactions on the substrate. Especially for the thickness window of cylinder-forming PS-*b*-PMMA-80, the more extensive compositional range of X_S from 0.48 to 0.85 as well as the larger thickness window in the vicinity of the neutral surfaces ($X_S \sim 0.64$) indicates that the greater the asymmetry of the PS-*b*-PMMA (the shorter PMMA), the greater is the tendency for the microdomain orientation normal to the neutral surfaces. This compositional asymmetry effect in BCP thin films on the microdomain orientation, significant in the thin films of highly asymmetric cylinder-forming PS-*b*-PMMA, might be dominantly correlated to the enhanced neutrality by the decrease of polymer density near surface favoring the perpendicular microdomain orientation on the neutral surfaces.

Acknowledgment. This work was supported by the Korea Research Foundation Grant (KRF-2007- D00230) and APCPI ERC program (R11-2007-050-01004) funded by the Ministry of Education, Science & Technology (MEST), Korea, the National Science Foundation under the MRSEC program (UCSB MRL, DMR-0520415 and UMASS, DMR-0213695), and the U.S. Department of Energy (DOE) under Contract DE-FG-0296ER45612.

References and Notes

(1) Hamley, I. W. *Nanotechnology* **2003**, *14*, R39.
(2) Hawker, C. J.; Russell, T. P. *MRS Bull.* **2005**, *30*, 952.
(3) Ruiz, R.; Kang, H.; Detcheverry, F. A.; Dobisz, E.; Kercher, D. S.; Albrecht, T. R.; de Pablo, J. J.; Nealey, P. F. *Science* **2008**, *321*, 936–939.
(4) Bita, I.; Yang, J. K. W.; Jung, Y. S.; Ross, C. A.; Thomas, E. L.; Berggren, K. K. *Science* **2008**, *321*, 939–943.
(5) Tang, C.; Lennon, E. M.; Fredrickson, G. H.; Kramer, E. J.; Hawker, C. J. *Science* **2008**, *322*, 429.
(6) Holden, G.; Legge, N. R.; Schroeder, H. E.; Quirk, R. P. *Thermoplastic Elastomers*; Hanser: New York, 1987.
(7) Bates, F. S.; Fredrickson, G. H. *Annu. Rev. Phys. Chem.* **1990**, *41*, 525.
(8) Hamley, I. W. *The Physics of Block Copolymers*; Oxford University Press: Oxford, 1998.
(9) Singh, C.; Pickett, G. T.; Zhulina, E.; Balazs, A. C. *J. Phys. Chem. B* **1997**, *101*, 10614.
(10) Fasolka, M. J.; Banerjee, P.; Mayes, A. M.; Pickett, G.; Balazs, A. C. *Macromolecules* **2000**, *33*, 5702.
(11) Guarini, K. W.; Black, C. T.; Yeung, S. H. I. *Adv. Mater.* **2002**, *14*, 1290.
(12) Jeong, U.; Ryu, D. Y.; Kho, D. H.; Kim, J. K.; Goldbach, J. T.; Kim, D. H.; Russell, T. P. *Adv. Mater.* **2004**, *16*, 533.
(13) Wang, H.; Djurisic, A. B.; Xie, M. H.; Chan, W. K.; Kutsay, O. *Thin Solid Films* **2005**, *488*, 329.
(14) Kitano, H.; Akasaka, S.; Inoue, T.; Chen, F.; Takenaka, M.; Hasegawa, H.; Yoshida, H.; Nagano, H. *Langmuir* **2007**, *23*, 6404.
(15) Russell, T. P.; Coulon, G.; Deline, V. R.; Miller, D. C. *Macromolecules* **1989**, *22*, 4600.
(16) Russell, T. P.; Menelle, A.; Anastasiadis, S. H.; Satija, S. K.; Majkrzak, C. F. *Macromolecules* **1991**, *24*, 6263.
(17) Pickett, G. T.; Balazs, A. C. *Macromolecules* **1997**, *30*, 3097.
(18) Kim, H.-C.; Russell, T. P. *J. Polym. Sci., Part B: Polym. Phys.* **2001**, *39*, 663.
(19) Khaydarov, A. A.; Hamley, I. W.; Legge, T. M.; Perrier, S. *Eur. Polym. J.* **2007**, *43*, 789.

(20) Mansky, P.; Liu, Y.; Huang, E.; Russell, T. P.; Hawker, C. J. *Science* **1997**, *275*, 1458.
(21) Huang, E.; Russell, T. P.; Harrison, C.; Chaikin, P. M.; Register, R. A.; Hawker, C. J.; Mays, J. *Macromolecules* **1998**, *31*, 7641.
(22) Ryu, D. Y.; Shin, K.; Drockenmuller, E.; Hawker, C. J.; Russell, T. P. *Science* **2005**, *308*, 236.
(23) In, I.; La, Y. H.; Park, S. M.; Nealey, P. F.; Gopalan, P. *Langmuir* **2006**, *22*, 7855.
(24) Ryu, D. Y.; Wang, J. Y.; Lavery, K. A.; Drockenmuller, E.; Satija, S. K.; Hawker, C. J.; Russell, T. P. *Macromolecules* **2007**, *40*, 4296.
(25) Han, E.; In, I.; Park, S.-M.; La, Y.-H.; Wang, Y.; Nealey, P. F.; Gopalan, P. *Adv. Mater.* **2007**, *19*, 4448.
(26) Bang, J.; Bae, J.; Löwenhielm, P.; Spiessberger, C.; Given-Beck, S. A.; Russell, T. P.; Hawker, C. J. *Adv. Mater.* **2007**, *19*, 4552.
(27) Ham, S.; Shin, C.; Kim, E.; Ryu, D. Y.; Jeong, U.; Russell, T. P.; Hawker, C. J. *Macromolecules* **2008**, *41*, 6431.
(28) Ji, S.; Liu, G.; Zheng, F.; Craig, G. S. W.; Himpsel, F. J.; Nealey, P. F. *Adv. Mater.* **2008**, *20*, 3054.
(29) Thurn-Albrecht, T.; DeRouchey, J.; Russell, T. P.; Jaeger, H. M. *Macromolecules* **2000**, *33*, 3250.
(30) Thurn-Albrecht, T.; DeRouchey, J.; Russell, T. P.; Kolb, R. *Macromolecules* **2002**, *35*, 8106.
(31) Xuan, Y.; Peng, J.; Cui, L.; Wang, H.; Li, B.; Han, Y. *Macromolecules* **2004**, *37*, 7301.
(32) Kim, S. H.; Misner, M. J.; Xu, T.; Kimura, M.; Russell, T. P. *Adv. Mater.* **2004**, *16*, 226.
(33) Kim, S. O.; Solak, H. H.; Stoykovich, M. P.; Ferrier, N. J.; de Pablo, J. J.; Nealey, P. F. *Nature (London)* **2003**, *424*, 411.
(34) Park, S. M.; S., M. P.; Ruiz, R.; Zhang, Y.; Black, C. T.; Nealey, P. F. *Adv. Mater.* **2007**, *19*, 607.
(35) Mansky, P.; Russell, T. P.; Hawker, C. J.; Pitsikalis, M.; Mays, J. *Macromolecules* **1997**, *30*, 6810.
(36) Huang, E.; Pruzinsky, S.; Russell, T. P.; Mays, J.; Hawker, C. J. *Macromolecules* **1999**, *32*, 5299.
(37) Han, E.; Stuen, K. O.; La, Y.-H.; Nealey, P. F.; Gopalan, P. *Macromolecules* **2008**, *41*, 9090.
(38) Hawker, C. J.; Elce, E.; Dao, J.; Volksen, W.; Russell, T. P.; Barclay, G. G. *Macromolecules* **1996**, *29*, 2686.
(39) Wang, Q.; Nealey, P. F.; de Pablo, J. J. *Macromolecules* **2001** ***34*, 3458.**
(40) Meng, D.; Wang, Q. *J. Chem. Phys.* **2007**, *126*, 234902.